Spontaneous dipolar Bose-Einstein condensation on the surface of a cylinder

Luis E. Young-S.[1,*] and S. K. Adhikari[2,†]

[1]*Grupo de Modelado Computacional y Programa de Matemáticas, Facultad de Ciencias Exactas y Naturales, Universidad de Cartagena, 130015 Cartagena de Indias, Bolivar, Colombia*
[2]*Instituto de Física Teórica, Universidade Estadual Paulista, 01.140-070 São Paulo, São Paulo, Brazil*

We demonstrate the spontaneous formation of a Bose-Einstein condensate (BEC) of strongly bound harmonically trapped dipolar ^{164}Dy atoms on the outer curved surface of an elliptical or a circular cylinder, with a distinct topology, employing the numerical solution of an improved mean-field model including a Lee-Huang-Yang-type interaction, meant to stop a collapse at high atom density, the axis of the cylindrical-shell-shaped BEC being aligned along the polarization direction of the dipolar atoms. These states are dynamically stable and a Gaussian initial state leads to the cylindrical-shell-shaped state in both imaginary-time and real-time propagation. The formation of the hollow cylindrical BEC by a real-time simulation starting from a solid cylindrical state demonstrate the possibility of the formation of such a condensate experimentally.

I. INTRODUCTION

After the experimental observation of a Bose-Einstein condensate (BEC) of alkali-metal atoms, this system has been the laboratory testing ground of different quantum phenomena, not accessible for experimental study previously. However, practically all of these studies were confined to a normal three-dimensional (3D) space or a two-dimensional (2D) plane or a one-dimensional straight line. Nevertheless, new physics may appear in curved spaces with distinct topology. Quantum states with distinct topology [1–4] have been the subject matter of intense investigation in recent times not only in search of new physics, but also due to its possible application in quantum information processing [5]. The nature of vortices on curved surfaces is, in general, different from the same in 3D space [6]. New types of vortices may appear in spinor condensates on a curved surface with distinct topology in synthetic gauge field [7,8]. Fractional quantum Hall states possess a richer structure evident through their response to topology [9]. Unique superfluid properties have been pointed out to exist in a BEC in a ring trap [10,11].

Consequently, in recent years there has been a great deal of interest in the investigation and the observation of a BEC on a curved surface with distinct topology and experimental studies have begun to investigate properties of a BEC formed on a spherical surface in the form of a spherical bubble. This is a difficult task in the presence of gravity, which will bring down the atoms from the top of the bubble. To circumvent this difficulty, there has been an attempt to create a single-species BEC of ^{87}Rb atoms on a spherical bubble in orbital microgravity [12] in a space-based quantum gas laboratory [13–15] following a suggestion [16,17] and elaborations in Refs. [18–21]. Optically trapped spherical-shell-shaped binary BEC of ^{23}Na and ^{87}Rb atoms in the immiscible phase has been created

and studied in a laboratory on earth [22], in the presence of gravity, following a suggestion [23,24] and consideration by others [25–27]. Hemispherical-shell-shaped BEC of ^{87}Rb atoms has also been created in a laboratory on earth [28] by a novel gravity compensation mechanism. All these experiments [12,22,28] for the creation of a spherical-shell-shaped BEC require a complex engineering of the external (confining) parameters. The same is true for a cylindrical-shell-shaped or a ring-shaped BEC created in a laboratory [10,11]. It is highly desirable to have a shell-shaped BEC in a *harmonic* trap with angular frequencies achievable in a laboratory.

In this paper we demonstrate the formation of a cylindrical-shell-shaped BEC of strongly dipolar ^{164}Dy atoms, with distinct topology in the form of a hollow cylinder, in a strong harmonic trap using an improved mean-field model including a Lee-Huang-Yang-type (LHY) interaction [29], appropriately modified for dipolar atoms [30–32], the axis of the cylinder being aligned along the polarization direction of dipolar atoms. Although a cylindrical shell is topologically equivalent to a ring, it has a different geometrical shape with an extended curved surface. This will allow study of new physics, like the emergence of a vortex and vortex lattice on a different curved surface. In the framework of the mean-field Gross-Pitaevskii (GP) equation, a dipolar BEC shows collapse instability as the dipolar interaction increases beyond a critical value [33,34] and the inclusion of a LHY interaction [30,32] in theoretical investigations stabilizes the dipolar condensate against collapse [35]. As the number of atoms N and/or the dipole moment of the atoms in a trapped quasi-2D dipolar BEC increases, the condensate cannot collapse due to the repulsive LHY interaction and, a droplet [33,34], or a spatially periodic [36] triangular-, square- [37], or honeycomb-lattice [37] structure of droplets or a labyrinthine state [38,39] could be formed in a strongly dipolar quasi-2D BEC. In a strong quasi-2D trap the formation of multiple droplets on a triangular lattice was confirmed in experiments [33,34,36] and substantiated in theoretical studies [37,40–43]. As the angular frequencies of

---

*lyoung@unicartagena.edu.co
†sk.adhikari@unesp.br, professores.ift.unesp.br/sk.adhikari/

the trap are further increased, the present cylindrical-shell-shaped BEC is formed as the number of atoms is increased beyond a critical value, where the dipolar atoms are deposited on the outer surface of a hollow cylinder.

The number of atoms, scattering length, and the trap parameters for the formation of a cylindrical-shell-shaped dipolar BEC of ^{164}Dy atoms are within the reach of ongoing experiments [44]. The scattering length a is taken in the range $85a_0 > a > 80a_0$, where a_0 is the Bohr radius. The frequency f_z of the harmonic trap in the polarization z direction is taken in the range 250 Hz $> f_z > 150$ Hz, whereas the frequencies f_x and f_y of the harmonic trap in the transverse x-y plane are taken as $f_x, f_y \approx 0.75 f_z$. We base our study on a numerical solution of an improved mean-field model, including the LHY interaction, by imaginary-time propagation. The number of atoms N is taken in the range $300\,000 > N > 100\,000$; in this study we take it to be mostly around $N \approx 200\,000$, as this number can easily be achieved in experiments with ^{164}Dy atoms [44,45]. For this choice of parameters, the only possible axially symmetric state is the cylindrical-shell-shaped state. Nevertheless, for $N \approx 200\,000$ and 150 Hz $< f_z \lesssim 250$ Hz, all Gaussian-type initial states lead to the cylindrical-shell-shaped state, in both imaginary- and real-time propagation. For $N \lesssim 100\,000$, single or multiple droplet states are preferentially formed. We find that, for $f_z \lesssim 120$ Hz, it is difficult to find a cylindrical-shell-shaped state numerically. As f_z is increased beyond 250 Hz the internal radius of the shell-shaped cylinder gradually decreases and eventually the cylindrical shell may become a solid cylinder and will not be discussed in this study. Moreover, we find that for large f_z ($f_z \gtrsim 210$ Hz) and large N ($N \gtrsim 330\,000$), one could have a cylindrical state with few (two to four) holes aligned parallel to the polarization direction (not studied here). If the ratio f_x/f_z is increased beyond 0.8, the internal radius of the cylindrical-shell-shaped state becomes smaller. However, as the ratio f_x/f_z is decreased beyond 0.7, although the internal radius of the cylindrical-shell-shaped state increases, it is not the ground state; droplet and multiple-droplet states naturally appear as the ground states as confirmed in previous experimental [33,34,36] and theoretical [37,40–43] studies. This is why, in this study of cylindrical-shell-shaped states, we will mostly consider $N \approx 200\,000$, 150 Hz $< f_z \lesssim 250$ Hz, $f_x, f_y = 0.75 f_z$, and $85a_0 > a > 80a_0$. If the confining harmonic trap in the x-y plane is made slightly anisotropic ($f_x \neq f_y$), the cylindrical shell of the strongly dipolar BEC becomes elliptical in nature.

For the experimental value of scattering length $a = 92a_0$ [46] of ^{164}Dy atoms, the atomic contact repulsion dominates over the dipolar interaction and the dipolar BEC has the form of a solid cylinder. As the scattering length is gradually reduced, the cylindrical-shell-shaped states appear. Starting from $a = 92a_0$, we demonstrate by real-time propagation that, as the scattering length is gradually reduced by a quasilinear ramp, the cylindrical-shell-shaped state appears for $a = 85a_0$ and the shell-shaped structure becomes more pronounced as the scattering length is reduced to $a = 80a_0$. This indicates the viability of the creation of a cylindrical-shell-shaped dipolar BEC in a laboratory by controlling the scattering length near a Feshbach resonance.

In Sec. II we present the improved mean-field model including the LHY interaction [29] appropriately modified

[30,32] for dipolar atoms with repulsive atomic interaction (positive scattering length). In Sec. III we present our numerical results for the formation of stationary cylindrical-shell-shaped dipolar BECs obtained by imaginary-time propagation. We also demonstrate the formation the cylindrical-shell-shaped states by real-time propagation starting from a cylindrically-symmetric Gaussian initial state. In Sec. IV we present a brief summary of our findings.

II. IMPROVED MEAN-FIELD MODEL

We consider a dipolar BEC of N atoms, polarized along the z direction, of mass m each, and with atomic scattering length a. The formation of a cylindrical-shell-shaped BEC can be formulated by the following 3D GP equation with the inclusion of the LHY interaction [47–50]:

$$
\begin{aligned}
i\hbar \frac{\partial \psi(\mathbf{r}, t)}{\partial t} = \Bigg[&-\frac{\hbar^2}{2m}\nabla^2 + U(\mathbf{r}) + \frac{4\pi\hbar^2}{m}aN|\psi(\mathbf{r}, t)|^2 \\
&+ \frac{3\hbar^2}{m}a_{\mathrm{dd}}N \int U_{\mathrm{dd}}(\mathbf{R})|\psi(\mathbf{r}', t)|^2 d\mathbf{r}' \\
&+ \frac{\gamma_{\mathrm{LHY}}\hbar^2}{m}N^{3/2}|\psi(\mathbf{r}, t)|^3 \Bigg]\psi(\mathbf{r}, t),
\end{aligned}
\tag{1}
$$

$$
U(\mathbf{r}) = \frac{1}{2}m(\omega_x^2 x^2 + \omega_y^2 y^2 + \omega_z^2 z^2),
\tag{2}
$$

$$
U_{\mathrm{dd}}(\mathbf{R}) = \frac{1 - 3\cos^2\theta}{|\mathbf{R}|^3}, \quad a_{\mathrm{dd}} = \frac{\mu_0\mu^2 m}{12\pi\hbar^2},
\tag{3}
$$

where $\omega_x(\equiv 2\pi f_x)$, $\omega_y(\equiv 2\pi f_y)$, $\omega_z(\equiv 2\pi f_z)$ are the angular frequencies of the harmonic trap along the x, y, z directions, respectively, μ_0 is the permeability of vacuum, μ is the magnetic dipole moment of each atom, $U_{\mathrm{dd}}(\mathbf{R})$ is the anisotropic dipolar interaction between two atoms located at $\mathbf{r} \equiv \{\mathbf{x}, \mathbf{y}, \mathbf{z}\}$ and $\mathbf{r}' \equiv \{\mathbf{x}', \mathbf{y}', \mathbf{z}'\}$, and θ is the angle made by $\mathbf{R} \equiv \mathbf{r} - \mathbf{r}'$ with the polarization z direction, and the dipolar length a_{dd} measuring the strength of atomic dipolar interaction in the same way as the scattering length a measures the strength of atomic contact interaction; the wave function is normalized as $\int |\psi(\mathbf{r}, t)|^2 d\mathbf{r} = 1$.

The LHY interaction coefficient γ_{LHY} in Eq. (1) is given by [30–32]

$$
\gamma_{\mathrm{LHY}} = \frac{128}{3}\sqrt{\pi a^5}Q_5(\varepsilon_{\mathrm{dd}}), \quad \varepsilon_{\mathrm{dd}} = \frac{a_{\mathrm{dd}}}{a},
\tag{4}
$$

where the auxiliary function $Q_5(\varepsilon_{\mathrm{dd}})$ includes the perturbative quantum-fluctuation correction due to dipolar interaction [30,32] and is given by

$$
Q_5(\varepsilon_{\mathrm{dd}}) = \int_0^1 dx(1 - \varepsilon_{\mathrm{dd}} + 3x^2\varepsilon_{\mathrm{dd}})^{5/2},
\tag{5}
$$

which can be approximated as [40,48]

$$
\begin{aligned}
Q_5(\varepsilon_{\mathrm{dd}}) = \frac{(3\varepsilon_{\mathrm{dd}})^{5/2}}{48}\Re\Bigg[&(8 + 26\eta + 33\eta^2)\sqrt{1+\eta} \\
&+ 15\eta^3 \ln\left(\frac{1 + \sqrt{1+\eta}}{\sqrt{\eta}}\right)\Bigg],
\end{aligned}
$$

$$
\eta = \frac{1 - \varepsilon_{\mathrm{dd}}}{3\varepsilon_{\mathrm{dd}}},
\tag{6}
$$

where Re denotes the real part. Limiting values are to be taken in Eq. (6) for $\varepsilon_{dd} = 0$ and 1, while $Q_5(0) = 1$ and $Q_5(1) = 3\sqrt{3}/2$ [40]. In this study we use the analytic expression (6) for $Q_5(\varepsilon_{dd})$. The dimensionless ratio ε_{dd} determines the strength of the dipolar interaction relative to the contact interaction and is useful to study many properties of a dipolar BEC. The perturbative result (4) is technically valid for $\varepsilon_{dd} < 1$, while $Q_5(\varepsilon_{dd})$ is real [30,32]. In the domain of the present study of strongly dipolar atoms ($\varepsilon_{dd} > 1$), $Q_5(\varepsilon_{dd})$ is complex. However, its imaginary part is negligible in comparison with its real part in the case of ^{164}Dy atoms [51] and will be neglected in this study as in other investigations [37,40,43,44].

Equation (1) can be written in the following dimensionless form if we scale lengths in terms of $l = \sqrt{\hbar/m\omega_z}$, time in units of ω_z^{-1}, angular frequency in units of ω_z, energy in units of $\hbar\omega_z$ and density $|\psi|^2$ in units of l^{-3}:

$$i\frac{\partial\psi(\mathbf{r},t)}{\partial t} = \left[-\frac{1}{2}\nabla^2 + \frac{1}{2}\left(f_x^2 x^2 + f_y^2 y^2 + z^2\right) \right.$$
$$+ 4\pi a N |\psi(\mathbf{r},t)|^2$$
$$+ 3 a_{dd} N \int U_{dd}(\mathbf{R})|\psi(\mathbf{r}',t)|^2 d\mathbf{r}'$$
$$\left. + \gamma_{LHY} N^{3/2}|\psi(\mathbf{r},t)|^3 \right]\psi(\mathbf{r},t), \qquad (7)$$

where all variables are scaled. We are using the same symbols to represent the scaled variables as the unscaled ones without any risk of confusion. Equation (7) can be derived using the variational principle

$$i\frac{\partial\psi}{\partial t} = \frac{\delta E}{\delta \psi^*}, \qquad (8)$$

which leads to the following energy functional corresponding to energy per atom:

$$E = \frac{1}{2}\int d\mathbf{r}\left[|\nabla\psi(\mathbf{r})|^2 + \left(f_x^2 x^2 + f_y^2 y^2 + z^2\right)|\psi(\mathbf{r})|^2 \right.$$
$$+ 3 a_{dd} N |\psi(\mathbf{r})|^2 \int U_{dd}(\mathbf{R})|\psi(\mathbf{r}')|^2 d\mathbf{r}'$$
$$\left. + 4\pi N a |\psi(\mathbf{r})|^4 + \frac{4\gamma_{LHY}}{5} N^{3/2}|\psi(\mathbf{r})|^5 \right] \qquad (9)$$

for a stationary state.

III. NUMERICAL RESULTS

To study the spontaneous condensation of dipolar ^{164}Dy atoms on the surface of a cylinder, the partial differential GP equation (7) is solved numerically using C/FORTRAN programs [49] or their open-multiprocessing versions [52,53], using the split-time-step Crank-Nicolson method by imaginary- and real-time propagation [54]. The imaginary-time propagation is employed to study the stationary states and the real-time propagation for dynamics. It is problematic to treat numerically the divergent $1/|\mathbf{R}|^3$ term in the dipolar potential (3) in configuration space. To avoid this problem the nonlocal dipolar interaction integral in the improved mean-field model

(7) is calculated in the momentum $\mathbf{k}$ space by a Fourier transformation employing the following convolution identity [49]

$$\int d\mathbf{r}' U_{dd}(\mathbf{R}) n(\mathbf{r}') = \int \frac{d\mathbf{k}}{(2\pi)^3} e^{-i\mathbf{k}\cdot\mathbf{r}} \widetilde{U}_{dd}(\mathbf{k}) \widetilde{n}(\mathbf{k}), \qquad (10)$$

where density $n(\mathbf{r}) \equiv |\psi(\mathbf{r})|^2$; $\widetilde{U}_{dd}(\mathbf{k})$ and $\widetilde{n}(\mathbf{k})$ are the Fourier transforms of the dipolar potential and density. The Fourier transformation of the dipolar potential $\widetilde{U}_{dd}(\mathbf{k})$ is analytically known [49] and this enhances the accuracy of the numerical procedure. The integrand in the right-hand side of Eq. (10) is a smooth function and can be evaluated numerically employing a fast Fourier transformation routine. In this way the problem is solved in momentum space and the solution in configuration space is obtained by taking another Fourier transformation.

For the appearance of a cylindrical-shell-shaped state, we need a strongly dipolar atom with $a_{dd} > a$. The system becomes repulsive for $a_{dd} < a$, and no such states can be formed. Although, $a_{dd} = 130.8a_0$ for ^{164}Dy atoms, we have a certain flexibility in fixing the scattering length a as the scattering length can be modified by the Feshbach resonance technique by manipulating an external electromagnetic field. In this study we take the scattering length $a = 80a_0$, whereas its experimental estimate is $a = (92 \pm 8)a_0$ [46]. With the reduction of contact repulsion, this choice of scattering length ($a = 80a_0$) has the advantage of slightly increasing the net attraction, which will facilitate the formation of pronounced cylindrical-shell-shaped BEC. For dysprosium atoms $m(^{164}$Dy$) \approx 164 \times 1.66054 \times 10^{-27}$ kg, $\hbar = 1.0545718 \times 10^{-34}$ m^2 kg/s. Consequently, for $f_z = 167$ Hz, 200 Hz, and 250 Hz, the units of length are $l = \sqrt{\hbar/m\omega_z} = 0.6075$ μm, 0.5551 μm, and 0.4965 μm, respectively. Incidentally, $f_z = 167$ Hz is the z frequency of the trap employed in the recent experiment on 2D supersolid formation in ^{164}Dy [36]. It is true that the frequency f_z is the same in both cases, but the quasi-2D trap shape in Ref. [36] is very different from the trap in the present case ($f_x, f_y = 0.75 f_z$), with much larger trap frequencies along the x and y directions, resulting in different configurations. The demonstration of a cylindrical-shell-shaped BEC is best confirmed by a hollow in the integrated 2D density $n_{2D}(x, y)$ defined by

$$n_{2D}(x, y) = \int_{-\infty}^{\infty} dz |\psi(x, y, z)|^2. \qquad (11)$$

The scenario of the formation of a cylindrical-shell-shaped state in a ^{164}Dy BEC is best illustrated by a phase plot of the number of atoms N versus trap frequency f_z, as obtained by imaginary-time propagation of Eq. (7) employing a cylindrically symmetric Gaussian initial state for $a = 80a_0$ and $f_x = f_y = 0.75 f_z$ as illustrated in Fig. 1. We find that, for a fixed f_z, the cylindrical-shell-shaped states are obtained for the number of atoms N larger than a critical value. For smaller f_z ($\lesssim 200$ Hz) and large N ($\gtrsim 3 \times 10^5$) one also has the labyrinthine states [38] (not studied here). To obtain the labyrinthine states, which are mostly excited states for $N < 300\,000$, special symmetry-broken initial states are needed in imaginary-time propagation. The cylindrically symmetric Gaussian initial states lead to the cylindrical-shell-shaped states. For smaller N ($\lesssim 10^5$), we find different states in the form of solid cylinders without any hollow part inside. These
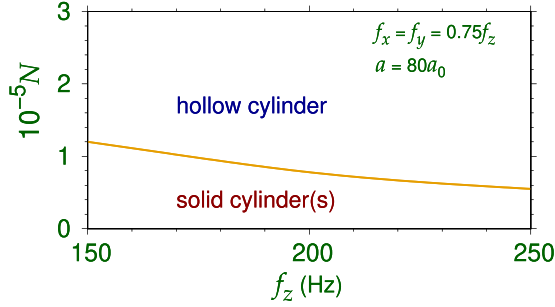
FIG. 1. Phase plot of number of atoms N versus trap frequency f_z illustrating the formation of a cylindrical-shell-shaped dipolar BEC of ^{164}Dy atoms. The region marked "solid cylinder(s)" include a single cylinder as well as multiple cylinders in the form of droplets.

include a single solid cylinder (not shown here) or multiple solid cylinders aligned along the z axis in the form of droplets, viz. Fig. 2(e).

A contour plot of the integrated 2D density $n_{2D}(x, y)$ of a cylindrical-shell-shaped state in a ^{164}Dy BEC is considered next. In Fig. 2(a), we illustrate a cylindrical-shell-shaped
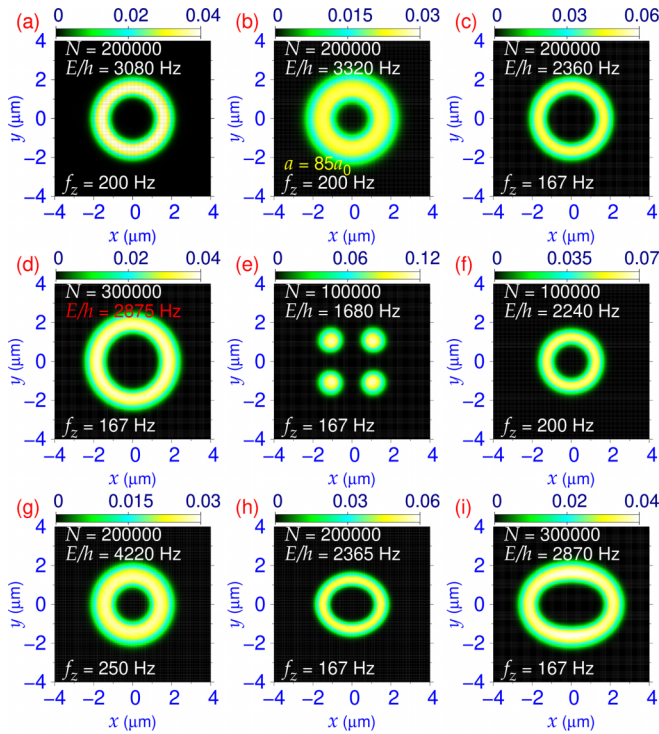

FIG. 2. Contour plot of dimensionless 2D density $n_{2D}(x, y)$ of four cylindrical-shell-shaped states of ^{164}Dy atoms ($a_{dd} = 130.8a_0$) for (a) $N = 200\,000$, $f_z = 200$ Hz, (b) $N = 200\,000$, $f_z = 200$ Hz, (c) $N = 200\,000$, $f_z = 167$ Hz, and (d) $N = 300\,000$, $f_z = 167$ Hz; that of a four-droplet state for (e) $N = 100\,000$, $f_z = 167$ Hz, those of two cylindrical-shell-shaped states for (f) $N = 100\,000$, $f_z = 200$ Hz, and (g) $N = 200\,000$, $f_z = 250$ Hz; that of a cylindrical-shell-shaped state with elliptical section for (h) $N = 200\,000$, $f_z = 167$ Hz, and (i) $N = 300\,000$, $f_z = 167$ Hz. In (a)–(g) $f_x = f_y = 0.75f_z$, and in (h)–(i) $f_x = 120$ Hz, and $f_y = 130$ Hz; in (b) $a = 85a_0$ and in (a) and (c)–(i) $a = 80a_0$. The energies per atom in each case appear in the E/h values in Hz displayed in respective plots.

state with $N = 200\,000$, $a = 80a_0$, $f_z = 200$ Hz, $f_x = f_y = 0.75f_z$. The inner radius of the cylindrical shell in Fig. 2(a) is quite sharp and pronounced. As the scattering length a is increased, the contact repulsion increases relative to the dipolar interaction and consequently, the inner radius of the cylindrical shell reduces as can be found in the contour plot of the cylindrical-shell-shaped state in Fig. 2(b) for $N = 200\,000$, $a = 85a_0$, $f_z = 200$ Hz, by comparing with the contour plot in Fig. 2(a) for $a = 80a_0$, with the other parameters unchanged. With the further increase of a, for $a \gtrsim 88a_0$, the cylindrical-shell-shaped state loses the shell-shaped structure and a Gaussian-type extended BEC in the shape of a normal solid cylinder is obtained in imaginary-time propagation (not explicitly shown here). On the other hand, as f_z is decreased, the inner radius of the cylindrical shell increases as can be found in the contour plot of the cylindrical-shell-shaped state in Fig. 2(c) for $N = 200\,000$, $a = 80a_0$, $f_z = 167$ Hz, by comparing with the contour plot in Fig. 2(a) for $f_z = 200$ Hz with other parameters unchanged. If the number of atoms N is increased, the inner radius of the cylindrical-shell-shaped state slightly increases as illustrated in the contour plot in Fig. 2(d) for $N = 300\,000$, $a = 80a_0$, $f_z = 167$ Hz, by comparing with the contour plot in Fig. 2(c) for $N = 200\,000$ with the other parameters unchanged. However, if N is decreased below a critical value, the cylindrical-shell-shaped states are not possible and only droplet states appear. For $f_z = 167$ Hz this happens for $N \approx 100\,000$ as illustrated in the contour plot of the four-droplet state in Fig. 2(e). For $f_z = 200$ Hz, this critical number is smaller and for $N = 100\,000$ a cylindrical-shell-shaped state appears, viz. Fig. 2(f). For $f_z = 200$ Hz, droplet states appear for $N \lesssim 75\,000$ (not displayed here). The inner radius of the cylindrical shell reduces further at an increased frequency $f_z = 250$ Hz as shown in plot in Fig. 2(g) for $N = 200\,000$, compare with plots in Figs. 2(a) and 2(c) for $f_z = 200$ Hz and $f_z = 167$ Hz, respectively. The circular section of the cylindrical-shell-shaped states becomes elliptical for an asymmetric trap in the $x - y$ plane ($f_x \neq f_y$) as demonstrated through the contour plot of $n_{2D}(x, y)$ in Fig. 2(h) for $N = 200\,000$ and (i) for $N = 300\,000$, and $a = 80a_0$, $f_z = 167$ Hz, $f_x = 120$ Hz, $f_y = 130$ Hz.

The extended hollow region of the cylindrical-shell-shaped state is best illustrated through the isodensity plot of the same. In Figs. 3(a) and 3(b) the side view and front view of the density $N|\psi(x, y, z)|^2$ are presented for the state with $N = 200\,000$, $a = 80a_0$, $f_z = 200$ Hz, viz. Fig. 2(a). In Figs. 3(c) and 3(d) the side view and front view of the density $N|\psi(x, y, z)|^2$ are presented for the state with $N = 200\,000$, $a = 80a_0$, $f_z = 167$ Hz, viz. Fig. 2(c). Finally, in Figs. 3(e) and 3(f) the side view and front view of the density $N|\psi(x, y, z)|^2$ are presented for the cylindrical-shell-shaped state with elliptic section for $N = 300\,000$, $a = 80a_0$, $f_z = 167$ Hz, viz. Fig. 2(i). Because of dipolar interaction the cylindrical-shell-shaped state is elongated in the polarization z direction. The length of the cylindrical shells is about 8 μm. However, in Figs. 3(a), 3(c), and 3(e) we show a section at $z = -4$ μm and -3 μm, so that the inner hollow region can be easily seen. The long inner hollow region of the cylinder, explicit in Figs. 3(b), 3(d), and 3(f) is also visible in the side view of Figs. 3(a), 3(c), and 3(f). The area of the internal hollow region has increased from Figs. 3(a) and 3(b) to Figs. 3(c) and
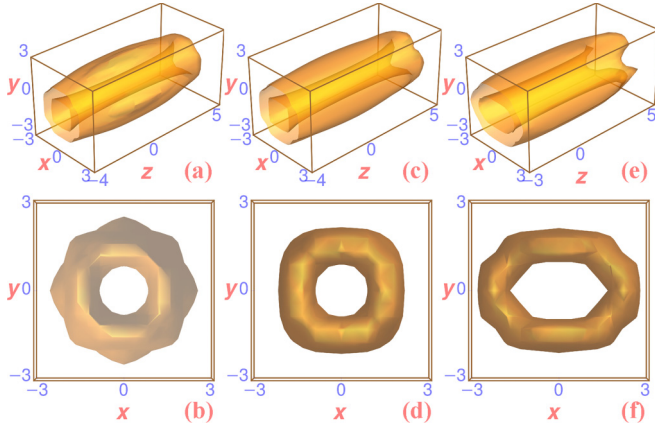
FIG. 3. (a) Side view and (b) front view of isodensity plot of $N|\psi(x,y,z)|^2$ of the cylindrical-shell-shaped state, viz. Fig. 2(a), of $N = 200\,000$ ^{164}Dy atoms in a trap with frequency $f_z = 200$ Hz. (c) Side view and (d) front view of the same, viz. Fig. 2(c), for $f_z = 167$ Hz and $N = 200\,000$. (e) Side view and (f) front view of the cylindrical-shell-shaped state with elliptic section, viz. Fig. 2(i), for $f_z = 167$ Hz and $N = 300\,000$. The unit of lengths x, y and z is μm. In plots (a)–(d) $f_x = f_y = 0.75 f_z$ and $a = 80a_0$ and in plots (e), (f) $f_x = 120$ Hz, $f_y = 130$ Hz, and $a = 80a_0$.
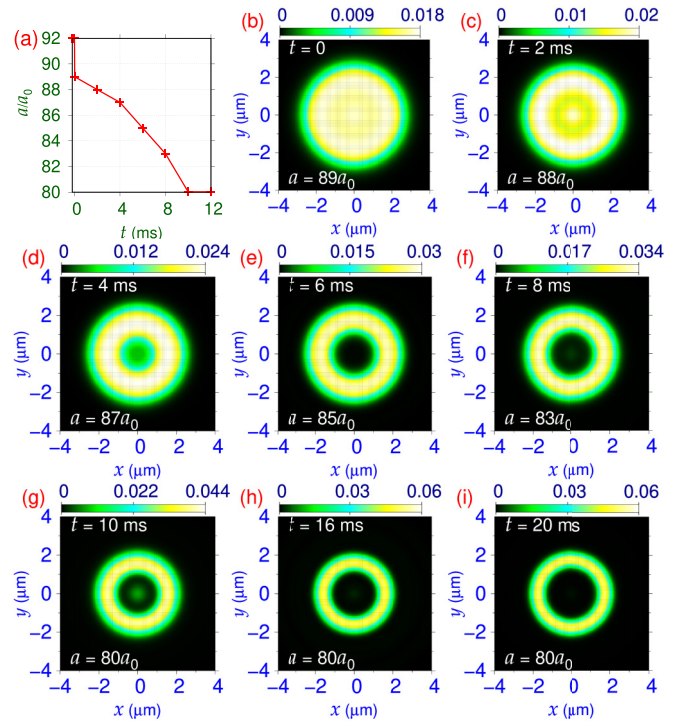

FIG. 4. Dynamical generation of a cylindrical-shell-shaped state of $N = 200\,000$ ^{164}Dy atoms of scattering length $a = 80a_0$ in a trap with frequencies $f_z = 167$ Hz, $f_x = f_y = 0.75 f_z$ by real-time propagation initiating from a converged cylindrical state of $N = 200\,000$ ^{164}Dy atoms of scattering length $a = 92a_0$ obtained by imaginary-time propagation in the same trap. (a) Scattering length versus time plot, the scattering length is changed once at an interval of 1 ms shown by the "plus" sign. Contour plot of 2D density $n_{2D}(x,y)$ in dimensionless units at (b) $t = 0 (a = 89a_0)$, (c) $t = 2$ ms ($a = 88a_0$), (d) $t = 4$ ms ($a = 87a_0$), (e) $t = 6$ ms ($a = 85a_0$), (f) $t = 8$ ms ($a = 83a_0$), (g) $t = 10$ ms ($a = 80a_0$), (h) $t = 16$ ms ($a = 80a_0$), (i) $t = 20$ ms ($a = 80a_0$).

3(d) due to a reduction of the trap frequency from $f_z = 200$ Hz to $f_z = 167$ Hz.

The cylindrical-shell-shaped states are very high density states, like the droplet states [33,34], the maximum density in the interior of the states in Fig. 2 is $\gtrsim 10^{15}$ atoms/cm^3, whereas the average density inside the state is about 3×10^{14} cm^{-3}. In this theoretical study we neglect the effect of three-body recombination loss of atoms. A matter of concern for the experimental observation [34,55] of a cylindrical-shell-shaped state is the large atom number ($N \sim 10^5$) required, where the effect of three-body recombination loss of atoms might not be negligible [42]. Nevertheless, a reasonably small value of the loss parameter ($= 1.25 \times 10^{-41}$ m^6/s) is estimated for ^{164}Dy atoms [34,56] from measurements on a thermal cloud and is assumed to be a constant over the small range of scattering lengths near $a = 80-90a_0$ close to the experimental estimate $a = 92a_0$ [46] and the value $a = 80a_0$ used in this study. The typical atomic density of 3×10^{14} cm^{-3} is within the acceptable limit for the formation of cylindrical-shell-shaped states in an experiment as established in previous experimental [34,56] and theoretical [42,55] investigations. A way to optimize the production of dipolar BECs with more than 2×10^5 atoms for the study of large-atom-number dipolar gases in the droplet and supersolid regimes has recently appeared in the literature [45].

The cylindrical shell-shaped states can possibly be easily realized in a laboratory. It is quite possible that, for the correct set of parameters, these high-density states would be naturally formed as in the case of the seven-droplet state on a triangular lattice [36]. Only an experiment can test this conjecture. Otherwise, they can be formed starting from a solid cylindrical state, naturally formed for the experimental value of scattering length $a (= 92a_0)$ [46] for $N = 200\,000$ ^{164}Dy atoms in a trap with frequency $f_z = 167$ Hz and $f_x = f_y = 0.75 f_z$, as we demonstrate here by real-time propagation starting

with the converged initial state obtained by imaginary-time propagation with $a = 92a_0$. During real-time propagation the scattering length a is changed at intervals of 2 ms to reach $a = 80a_0$ at 10 ms, via $a = 89a_0$ at $t = 0$, $a = 88a_0$ at $t = 2$ ms, $a = 87a_0$ at $t = 4$ ms, $a = 85a_0$ at $t = 6$ ms, $a = 83a_0$ at $t = 8$ ms, and $a = 80a_0$ at $t = 10$ ms. This time variation of the scattering length is displayed in Fig. 4(a). The contour plot of 2D density $n_{2D}(x,y)$ as obtained in real-time propagation is illustrated in Figs. 4(b) to 4(i) at times $t = 0$, $t = 2$ ms, $t = 4$ ms, $t = 6$ ms, $t = 8$ ms, $t = 10$ ms, $t = 16$ ms, and $t = 20$ ms. We find that the hollow region has been created at $t = 6$ ms starting from a solid cylinder at $t = 0$. This hollow region keeps on oscillating radially for $t > 10$ ms and eventually settles to its equilibrium value at large times.

IV. SUMMARY

The importance of the study of quantum states with distinct topology cannot be overemphasized [1–3]. However, the generation of such states requires an engineering of different control parameters as in the recent experiments with a spherical-shell-shaped [12,22,28] and ring-shaped [10,11]

BEC. In this paper, we demonstrated the possibility of the formation of high-density dynamically stable cylindrical-shell-shaped quantum states with distinct topology in a harmonically trapped dipolar BEC of ^{164}Dy atoms for parameters (number of atoms, trap frequencies) employed in the recent experiments [44], using an improved mean-field GP model including the LHY interaction [29] appropriately modified for dipolar atoms [30–32]. We demonstrated by real-time simulation that, starting from an initial state with the shape of a solid cylinder at $a = 92a_0$, and by ramping down the scattering length in a few steps to the desired value ($a = 80a_0$) in a short interval of time ($\sim$10 ms), it is possible to generate the cylindrical-shell-shaped state quickly. This ensures the possibility of observing a cylindrical-shell-shaped state in a laboratory in a harmonically trapped dipolar BEC of ^{164}Dy atoms in the near future.

[1] M. Z. Hasan and C. L. Kane, Rev. Mod. Phys. **82**, 3045 (2010).

[2] X.-L. Qi and S.-C. Zhang, Rev. Mod. Phys. **83**, 1057 (2011).

[3] C.-K. Chiu, J. C. Y. Teo, A. P. Schnyder, and S. Ryu, Rev. Mod. Phys. **88**, 035005 (2016).

[4] N. S. Móller, F. E. A. dos Santos, V. S. Bagnato, and A. Pelster, New J. Phys. **22**, 063059 (2020).

[5] A. Stern and N. H. Lindner, Science **339**, 1179 (2013).

[6] A. M. Turner, V. Vitelli, and D. R. Nelson, Rev. Mod. Phys. **82**, 1301 (2010).

[7] T.-L. Ho and B. Huang, Phys. Rev. Lett. **115**, 155304 (2015).

[8] N.-E. Guenther, P. Massignan, and A. L. Fetter, Phys. Rev. A **96**, 063608 (2017).

[9] T. Can, M. Laskin, and P. Wiegmann, Phys. Rev. Lett. **113**, 046803 (2014).

[10] S. Moulder, S. Beattie, R. P. Smith, N. Tammuz, and Z. Hadzibabic, Phys. Rev. A **86**, 013629 (2012).

[11] S. Eckel, J. G. Lee, F. Jendrzejewski, N. Murray, C. W. Clark, C. J. Lobb, W. D. Phillips, M. Edwards, and G. K. Campbell, Nature (London) **506**, 200 (2014).

[12] R. A. Carollo, D. C. Aveline, B. Rhyno, S. Vishveshwara, C. Lannert, J. D. Murphree, E. R. Elliott, J. R. Williams, R. J. Thompson, and N. Lundblad, Nature (London) **606**, 281 (2022).

[13] D. C. Aveline, J. R. Williams, E. R. Elliott, C. Dutenhoffer, J. R. Kellogg, J. M. Kohel, N. E. Lay, K. Oudrhiri, R. F. Shotwell, N. Yu, and R. J. Thompson, Nature (London) **582**, 193 (2020).

[14] N. Gaaloul, M. Meister, R. Corgier, A. Pichery, P. Boegel, W. Herr, H. Ahlers, E. Charron, J. R. Williams, R. J. Thompson, W. P. Schleich, E. M. Rasel, and N. P. Bigelow, Nat. Commun. **13**, 7889 (2022).

[15] A. Bassi, L. Cacciapuoti, S. Capozziello, S. Dell'Agnello, E. Diamanti, D. Giulini, L. Iess, P. Jetzer, S. K. Joshi, A. Landragin, C. Le Poncin-Lafitte, E. Rasel, A. Roura, C. Salomon, and H. Ulbricht, npj Microgravity **8**, 49 (2022).

[16] O. Zobay and B. M. Garraway, Phys. Rev. Lett. **86**, 1195 (2001).

[17] O. Zobay and B. M. Garraway, Phys. Rev. A **69**, 023605 (2004).

[18] K. Sun, K. Padavić, F. Yang, S. Vishveshwara, and C. Lannert, Phys. Rev. A **98**, 013609 (2018).

[19] S. K. Adhikari, Phys. Rev. A **85**, 053631 (2012).

[20] M. Meister, A. Roura, E. M. Rasel, and W. P. Schleich, New J. Phys. **21**, 013039 (2019).

[21] A. Tononi and L. Salasnich, Phys. Rev. Lett. **123**, 160403 (2019).

[22] F. Jia, Z. Huang, L. Qiu, R. Zhou, Y. Yan, and D. Wang, Phys. Rev. Lett. **129**, 243402 (2022).

[23] T.-L. Ho and V. B. Shenoy, Phys. Rev. Lett. **77**, 3276 (1996).

[24] H. Pu and N. P. Bigelow, Phys. Rev. Lett. **80**, 1130 (1998).

[25] M. Trippenbach, K. Góral, K. Rzazewski, B. Malomed, and Y. B. Band, J. Phys. B **33**, 4017 (2000).

[26] K. L. Lee, N. B. Jorgensen, I. Kang Liu, L. Wacker, J. J. Arlt, and N. P. Proukakis, Phys. Rev. A **94**, 013602 (2016).

[27] A. Wolf, P. Boegel, M. Meister, A. Balaž, N. Gaaloul, and M. A. Efremov, Phys. Rev. A **106**, 013309 (2022).

[28] Y. Guo, E. Mercado Gutierrez, D. Rey, T. Badr, A. Perrin, L. Longchambon, V. S. Bagnato, H. Perrin, and R. Dubessy, New J. Phys. **24**, 093040 (2022).

[29] T. D. Lee, K. Huang, and C. N. Yang, Phys. Rev. **106**, 1135 (1957).

[30] A. R. P. Lima and A. Pelster, Phys. Rev. A **84**, 041604(R) (2011).

[31] A. R. P. Lima and A. Pelster, Phys. Rev. A **86**, 063609 (2012).

[32] R. Schützhold, M. Uhlmann, Y. Xu, and U. R. Fischer, Int. J. Mod. Phys. B **20**, 3555 (2006).

[33] H. Kadau, M. Schmitt, M. Wenzel, C. Wink, T. Maier, I. Ferrier-Barbut, and T. Pfau, Nature (London) **530**, 194 (2016).

[34] M. Schmitt, M. Wenzel, F. Böttcher, I. Ferrier-Barbut, and T. Pfau, Nature (London) **539**, 259 (2016).

[35] F. Wächtler and L. Santos, Phys. Rev. A **93**, 061603(R) (2016).

[36] M. A. Norcia, C. Politi, L. Klaus, E. Poli, M. Sohmen, M. J. Mark, R. Bisset, L. Santos, and F. Ferlaino, Nature (London) **596**, 357 (2021).

[37] L. E. Young-S. and S. K. Adhikari, Phys. Rev. A **105**, 033311 (2022).

[38] J. Hertkorn, J.-N. Schmidt, M. Guo, F. Böttcher, K. S. H. Ng, S. D. Graham, P. Uerlings, T. Langen, M. Zwierlein, and T. Pfau, Phys. Rev. Res. **3**, 033125 (2021).

[39] A. J. Dickstein, S. Erramilli, R. E. Goldstein, D. P. Jackson, and S. A. Langer, Science **261**, 1012 (1993).

[40] E. Poli, T. Bland, C. Politi, L. Klaus, M. A. Norcia, F. Ferlaino, R. N. Bisset, and L. Santos, Phys. Rev. A **104**, 063307 (2021).

[41] D. Baillie and P. B. Blakie, Phys. Rev. Lett. **121**, 195301 (2018).

[42] Y.-C. Zhang, T. Pohl, and F. Maucher, Phys. Rev. A **104**, 013310 (2021).

[43] L. E. Young-S. and S. K. Adhikari, Eur. Phys. J. Plus **137**, 1153 (2022).

[44] L. Chomaz, I. Ferrier-Barbut, F. Ferlaino, B. Laburthe-Tolra, B. L. Lev, and T. Pfau, Rep. Prog. Phys. **86**, 026401 (2023).

[45] M. Krstajić, P. Juhász, J. Kučera, L. R. Hofer, G. Lamb, A. L. Marchant, and R. P. Smith, arXiv:2307.01245 [Phys. Rev. A (to be published)].

[46] Y. Tang, A. Sykes, N. Q. Burdick, J. L. Bohn, and B. L. Lev, Phys. Rev. A **92**, 022703 (2015).

[47] T. Lahaye, C. Menotti, L. Santos, M. Lewenstein, and T. Pfau, Rep. Prog. Phys. **72**, 126401 (2009).

[48] R. N. Bisset, R. M. Wilson, D. Baillie, and P. B. Blakie, Phys. Rev. A **94**, 033619 (2016).

[49] R. K. Kumar, L. E. Young-S., D. Vudragović, A. Balaž, P. Muruganandam, and S. K. Adhikari, Comput. Phys. Commun. **195**, 117 (2015).

[50] V. I. Yukalov, Laser Phys. **28**, 053001 (2018).

[51] L. E. Young-S. and S. K. Adhikari, Commun. Nonlin. Sci. Numer. Simul. **115**, 106792 (2022).

[52] L. E. Young-S., P. Muruganandam, A. Balaž, and S. K. Adhikari, Comput. Phys. Commun. **286**, 108669 (2023).

[53] V. Lončar, L. E. Young-S., S. Škrbić, P. Muruganandam, S. K. Adhikari, and A. Balaž, Comput. Phys. Commun. **209**, 190 (2016).

[54] P. Muruganandam and S. K. Adhikari, Comput. Phys. Commun. **180**, 1888 (2009).

[55] Y.-C. Zhang, F. Maucher, and T. Pohl, Phys. Rev. Lett. **123**, 015301 (2019).

[56] I. Ferrier-Barbut, H. Kadau, M. Schmitt, M. Wenzel, and T. Pfau, Phys. Rev. Lett. **116**, 215301 (2016).